On-Line Supplementary Information

Multicolored Nanometer-Resolution Mapping of Single Protein-Ligand Binding Complexes Using Far-Field Photostable Optical Nanoscopy (PHOTON)

Tao Huang and Xiao-Hong Nancy Xu*

Department of Chemistry and Biochemistry, Old Dominion University, Norfolk, VA 23529

The on-line supplementary information includes:

(A) Materials and Methods

(B) Seven Supplementary Figures and Figure Caption

Fig. S1: Characterization of sizes and plasmonic optical properties of single Ag NPs

Fig. S2: NMR characterization of functional groups attached on the surface of Ag NPs.

Fig. S3: Characterization of binding activities of SMNOBS (AgMMUA-Biotin NPs)

Fig. S4: Mapping of centroids of three SMNOBS bound with single streptavidin molecules in biotin-streptavidin complexes using deconvolution and point spread function (PSF).

Fig. S5: Nanometer-Resolution imaging of three SMNOBS bound with single streptavidin molecules in single biotin-streptavidin complexes using PHOTON.

Fig. S6: Mapping of centroids of two SMNOBS bound with single streptavidin molecules in single biotin-streptavidin complexes using deconvolution and PSF.

Fig. S7: Nanometer-Resolution imaging of two SMNOBS bound with single streptavidin molecules in single biotin-streptavidin complexes using PHOTON.

* To whom correspondence should be addressed: Email: xhxu@odu.edu; www.odu.edu/sci/xu/xu.htm; Tel/fax: (757) 683-5698

A. Materials and Methods

Reagents and Supplies

Sodium borohydride (≥ 98%), sodium citrate dihydrate (≥ 99%), silver nitrate (≥ 99.9%), hydrogen peroxide (30%), polyvinylpyrrolidone (PVP), 11-mercaptoundecanoic acid (MUA ≥ 95%), 6-mercapto-1-hexanol (MCH) (≥ 97%), (+)-biotinamidohexanoic acid hydrazide (biotin-AHH) (95%), and streptavidin were purchased from Sigma-Aldrich. *N*-hydroxysulfosuccinimide (Sulfo-NHS ≥ 98.5%) and 1-Ethyl-3-[3-dimethylaminopropyl]-carbodiimide hydrochloride (EDC ≥ 99%) were purchased from Pierce. Nanopure deionized water (DI, 18 MΩ, Barnstead) was used to rinse glassware for synthesis of Ag nanoparticles (NPs) and to prepare all solutions, including 10 mM phosphate buffer saline (PBS) (pH = 7.4, 10 mM of phosphate buffer and NaCl).

Synthesis and Characterization of SMNOBS (AgMMUA-Biotin)

2.6 ± 1.1 nm Ag NPs

We synthesized and characterized Ag NPs with average diameters of 2.6 ± 1.1 nm and functionalized Ag NPs with a mixed monolayer of MUA and MCH, as we described previously.[1-2] Briefly, $AgNO_3$ (0.11 mM), sodium citrate (1.91 mM), PVP (0.052 mM), and H_2O_2 (25.0 mM) in nanopure DI water (42.3 mL) were prepared freshly and well mixed under stirring. $NaBH_4$ (150 μL, 100 mM) was added into the mixture, which was stirred for another 3 h to synthesize Ag NPs. The solution was filtered using 0.2 μm membrane filters, and immediately used for characterization and for preparation of AgMMUA NPs. TEM samples of Ag NPs were characterized using high-resolution transmission electron microscopy (HRTEM) (JEOL JEM-2100F), showing diameters of Ag NPs at 2.6 ± 1.1 nm (Fig. S1). The Ag NP solution was also immediately characterized using our dark-field optical microscopy and

spectroscopy (DFOMS, also named as SNOMS by us), UV-vis spectroscopy (Hitachi U3310), and dynamic light scattering (DLS) (Nicomp 380ZLS particle sizing system). Concentration of Ag NPs was calculated as 154 nM, using the same approaches as we reported previously. [3-7]

We have fully described the design and construction of our DFOMS for real-time imaging and spectroscopic characterization of single NPs in solutions,[3, 8-10] in single living cells, [1, 7, 11-16] and in single zebrafish embryos.[3, 8-9] In this study, dark-field optical microscope is equipped with a dark-field condenser (Oil 1.43-1.20, Nikon), a microscope illuminator (Halogen lamp, 100 W), and a 100x objective (Nikon Plan fluor 100x oil, SL. N.A. 0.5-1.3, W.D. 0.20 mm). The microscope is coupled with Nuance Multispectral Imaging System (N-MSI-VIS-FLEX, CRI), CCD camera equipped with liquid-crystal tunable filter (LCTF).[17]

AgMMUA NPs

AgMMUA NPs were prepared by mixing MUA (10 mM) and MCH (90 mM) in ethanol with freshly prepared Ag NPs (50 mL, 154 nM) to have final concentrations of MUA, MCH and Ag NPs at 0.1 mM, 0.9 mM, and 152 nM, respectively.[1, 11] The solutions were then stirred for 24 h to attach MUA and MCH onto the surface of NPs via the interaction of –SH groups with NPs and SN2 replacement reaction of citrate molecules with MUA and MCH (Fig. 2A in main text). The AgMMUA NPs were washed twice using nanopure DI water to remove excess MUA and MCH using centrifugation (Beckman Optima L90k, 50 Ti rotor, 30,000 rpm at 4°C for 60 min), and immediately characterized using DFOMS, UV-vis spectroscopy, and DLS.

Notably, the attached functional groups (MUA and MCH) on the surface of NPs changed the dielectric constant of NP, which led to the red shift of LSPR spectra of Ag NPs, from blue color to green colors, as shown in Figures S1-D and 2E. The yields of preparation of AgMMUA NPs from Ag NPs were characterized using DFOMS at single NP resolution and

using UV-vis spectroscopy for bulk NP solution. The results show the average yield of 92.0 ± 0.8, which confirms the superior strong interaction of –SH group of MUA and MCH with the surface of Ag NPs.

NMR samples of AgMMUA were immediately prepared by drying the washed AgMMUA NPs using lyophilizer (VirTis) and dissolving AgMMUA NPs (50 mg) in D_2O (1 mL), and further characterized using NMR (400 MHz, Bruker). NMR spectra in Fig. 2S show molar ratio of citrate : MCH : MUA : PVP = 33 : 5 :1 :0.03. One MUA per NPs was determined by a close-packing model, as we described previously. [1]

AgMMUA-Biotin NPs (SMNOBS)

We used a two-step method to conjugate the carboxyl group of AgMMUA with amine group of biotin-AHH via a peptide bond using EDC and sulfo-NHS as mediators (Fig. 2B in the text). EDC (77 μmol) and sulfo-NHS (7.7 μmol) were added to AgMMUA aqueous solution (50 mL, 154 nM), forming AgMMUA-s-NHS esters. After stirring at room temperature for 40 min, the AgMMUA-s-NHS was isolated using a Centriprep YM-30 (Millipore) by centrifugation at 1500 rcf (relative-centrifuge-force) for 5 min to remove excess EDC and sulfo-NHS, and then re-dissolved in the PBS buffer.

In the second step, biotin-AHH was added to AgMMUA-s-NHS in the buffer at a molar ratio of biotin to AgMMUA of 0.97. The solution was mixed using a rotary shaker at room temperature for 2 h and then at 4 ºC for 12 h. The AgMMUA-Biotin NPs were washed using the PBS buffer (10 mM) to remove excess biotin-AHH using centrifugation. The pellet was resuspended in the buffer, which was characterized using DFOMS, UV-vis spectroscopy, and DLS. Each AgMMUA NP could only conjugate with one biotin molecule to create SMNOBS,

because only one carboxyl group is available per AgMMUA NP, as characterized by NMR spectra (Fig. S2) and a close-packing model, as we described previously.[1] Thus, one AgMMUA-biotin NP (SMNOBS) has only one biotin molecule, which can be used to track its binding with a single streptavidin molecule and to map its individual binding sites in individual protein-ligand (streptavidin-biotin) complexes.

AgMMUA-Biotin-Streptavidin NPs

To determine the possible steric effects of NPs on the binding affinity of biotin with streptavidin, we measured the binding constant (affinity) of AgMMUA-Biotin NPs with streptavidin in the PBS buffer by measuring the absorbance of AgMMUA-Biotin NPs (60 nM) incubated with streptavidin (600 nM) over time.[1, 11] The UV-vis absorption spectra were measured at room temperature every 5 min for the first 2 h and at every 2.5-25 h after that until 48 h. The mixture was stored at 4 ºC between each spectroscopy measurement.

UV-vis absorption spectra of AgMMUA-Biotin NPs show stable peak wavelengths at 403 ± 1 nm (Fig. S3A) with the extinction coefficient (molar absorptivity, ε) of 9.5×10^6 $M^{-1}cm^{-1}$, which was determined by the Beer-Lambert Law with a dilution series of AgMMUA-Biotin NPs solutions. As AgMMUA-Biotin NPs were incubated with Streptavidin, absorbance of the spectra decreased over incubation time with its peak wavelength (403 nm) and FWHM remaining essentially unchanged (Fig. S3A), suggesting that AgMMUA-Biotin-Streptavidin NPs did not contribute significantly to the absorption. Such interesting phenomena might be attributable to the decrease of reflectivity of NPs due to the surface functional molecules, leading to the decrease of scattering and absorption intensity.[1, 11]

The results further confirm one biotin molecule per NP and the successful preparation of SMNOBS. Otherwise, if there were multiple biotin molecules per NP, one NP can bind with

more than one streptavidin molecule, which would lead to the aggregation of NPs and the red shift of UV-vis absorption spectrum.

A plot of the peak absorbance subtracted from baseline versus time in Fig. S3B exhibits high linearity during the first 30 min of the incubation time (Fig. S3C) and then remains constant, suggesting that the binding of SMNOBS with streptavidin is a first-order reaction, as those we calculated previously.[11] Binding constant (3.2×10^{15}) and associate rate constant ($6 \times 10^{2}\ M^{-1}s^{-1}$) are calculated using the approaches as we described previously,[1, 11] which agrees well with those reported in the literature.[18-20] The result in Fig. S3 demonstrates that the biotin conjugated with AgMMUA maintains its affinity and no steric effects of Ag NPs are observed.

Characterization of Photostability of SMNOBS

Photostability of single AgMMUA-Biotin NPs (SMNOBS) was characterized, using the same approach as we described previously.[1, 9] Sequential optical images of single SMNOBS were acquired using dark-field optical microscope equipped with MSIS, with exposure time of 100 ms and readout time of 40.6 ms, while these NPs were constantly irradiated under a dark-field microscope illuminator (100 W halogen) for 14 h.[1, 9] The illumination power at the sample stage (focal plane of dark field) was (0.070 ± 0.001) Watt during the experiment. Scattering intensity of individual NPs was measured over time to determine their photostability (Fig. 2D), showing that SMNOBS exhibits superior photostability (non-bleaching and non-blinking). More than 100 of SMNOBS were characterized to gain sufficient statistics to represent the bulk SMNOBS in solution at single NP resolution.

Design and Data Analysis of PHOTON for Nanometer-Resolution Imaging of Single Biotin Molecules and their Binding Sites in Single Biotin-Streptavidin Complexes

Stacks of the plasmonic images (image cubes) of single AgMMUA-Biotin-Streptavidin NPs were acquired from 420 to 720 nm at each nm (1 nm spectral resolution) with 100 ms exposure time using Multispectral Imaging System (MSIS; CCD camera equipped with LCTF), as shown in Figs. 3A, S4A, S6A. The LSPR spectra of AgMMUA-Biotin-Streptavidin NPs were deconvoluted using individual LSPR spectrum of single SMNOBS via Cauchy-Lorentz distribution model (Figs. 3C, S4C, S6C), as described in Eq. [S1]. [21-24]

$$I(\lambda) = \sum_{i=1}^{n} \frac{a_i}{\left[1 + \left(\frac{\lambda - \lambda_i}{b_i}\right)^2\right]} \qquad [S1]$$

Where n is the total number of individual SMNOBS (AgMMUA-Biotin NPs), I(λ) is the scattering intensity of single NP clusters (AgMMUA-Biotin-Streptavidin NPs) at a given wavelength (λ), a_i is the peak intensity of the i^{th} NPs, λ_i is the peak wavelength (λ_{max}) of the i^{th} NPs, and b_i is the half of the FWHM of the LSPR spectrum of the i^{th} NPs.

Using Matlab curve fitting tools with the customized Eq. [S1], each spectrum of the NP clusters, as circled in Fig. 3A, was fitted. The range of a_i from 0 to infinity, the range of λ_i from 510 to 600 nm (based upon range of λ_{max} of LSPR spectra of all individual SMNOBS in Fig. 2E), and range of b_i from 25 to 45 (based upon FWHM of LSPR spectra of SMNOBS in Fig. 2E), were set for fitting the curves (spectra). The total number of single NPs in each cluster was determined by the best fitting curve of the spectrum. The fitting curves with different n values were compared and the best fitting curve with the highest regression (R^2) was selected.

The LSPR spectrum of each NP (SMNOBS) can then be described by Eq. [S2]:

$$I_i(\lambda) = \frac{a_i}{\left[1 + (\frac{\lambda - \lambda_i}{b_i})^2\right]} \quad [S2]$$

Where $I_i(\lambda)$ is scattering intensity of the i^{th} NP at a given wavelength (λ). Notably, a_i, λ_i and b_i were determined by the spectral curve fitting using Eq. [S1], as described above.

Using the LSPR spectra of single SMNOBS (Figs. 3C: a-d; S2: a-c and S6: a-b) obtained from Eq. [S2], the image cubes of the NP clusters, as those shown in Fig. 3A, were unmixed (deconvoluted) at the given wavelength of each NP. For n number of NPs, n images were generated in TIFF format. Each image is the profile of scattering intensity of a single NP with the corresponding LSPR spectrum versus its location in the full frame of CCD array, as shown in Figs. 3D, S4D, and S6D.

The deconvolution (un-mixing) of each image cube was performed as described below using the software of MSIS, as each image cube of the NP clusters at each pixel is made up of a linear combination of LSPR spectra of individual NPs at the pixel. [25]

$$\mathbf{S}_{x,y} = L\mathbf{w} \quad [S3]$$

$$S_{x,y} = \begin{bmatrix} L_{11} & L_{12} & \dots & L_{1n} \\ L_{21} & L_{22} & \dots & L_{2n} \\ \dots & \dots & & \dots \\ L_{m1} & L_{m2} & \dots & L_{mn} \end{bmatrix} \begin{bmatrix} w_1 \\ w_2 \\ \dots \\ w_n \end{bmatrix} \quad [S4]$$

Where $\mathbf{S}_{x,y}$ is a vector containing multiple LSPR spectra at each pixel; L is a matrix with n LSPR spectra from n number of single NPs, m is the number of spectral channels, and **w** is vector of scattering intensity contributed by each NP in L matrix for each pixel in each image.

Here L_{ji} is the scattering intensity, $I_i(j+419)$, of the i^{th} NP at the j^{th} channel (wavelength, $\lambda = j + 419$ nm, ranging from 420 to 720 nm, totally m of 301 channels). For example, L_{11}, L_{21}, … L_{m1} represents scattering intensity of the LSPR spectrum of the 1^{st} NP, and L_{1n} L_{2n} … L_{mn} represents scattering intensity of the LSPR spectrum of the n^{th} NP.

Note that w_i is the percent of scattering intensity of i^{th} NPs in total scattering intensity contributed by total number (n) of NPs in each pixel, as described in Eq. [S5].

$$I_{i,x,y}(\lambda) = w_i I_{x,y}(\lambda) \quad [S5]$$

Where $I_{i,x,y}(\lambda)$ is scattering intensity of the i^{th} NPs at a given wavelength (λ) in a pixel located in (x, y). $I_{x,y}(\lambda)$ is total scattering intensity of n NPs (undeconvoluted NP clusters) at the same given wavelength in the same pixel. Thus, sum of w_i ($w_1 + w_2 + \ldots + w_n$) is equal to one.

The least squares approximation was used to minimize the residuals (*e*) and to obtain the best values of **w,** as described below in Eq. [S6].

$$e = \left\| Lw - S_{x,y} \right\|^2 \quad [S6]$$

After deconvolution (unmixed) of each image cube, a grayscale image in TIFF format for each NP with a given LSPR spectrum was generated. The image of each NP was then fitted by PSF using 2D Gaussian distribution (Figs. 3D, S4D, S5D), as described in Eq. [S7].[26]

$$N_{x,y} = B + N_{00} e^{-\frac{1}{2}\left[\left(\frac{x-x_0}{S_x}\right)^2 + \left(\frac{y-y_0}{S_y}\right)^2 \right]} \quad [S7]$$

Where (x_0, y_0) is centroid of a scattering point; $N_{x,y}$ is scattering intensity of a NP at the pixel (x, y); N_{00} is scattering intensity at the centroid (x_0, y_0); S_x and S_y are the widths of the PSF in x and y directions, respectively; and B is background intensity.

Center positions of the 2D-Gaussian fittings are the precise locations (centroids) of each NP. The standard deviations (SD) of the centroids were determined using FWHM of 2D-Gaussian fitting curves, as described in Eq. [S8]:

$$SD = \frac{FWHM}{2\sqrt{2\ln 2}} \approx \frac{FWHM}{2.355} \qquad [S8]$$

Using the same approaches, twenty image cubes (stack images of plasmonic images of NP clusters at each wavelength from 420-720 nm with 1-nm resolution) were taken and twenty precise locations for each NP were analyzed, as described above and shown in Figs. 4A, S5A and S7A. The 20 precise locations of each NP were then fitted by 2D-Gaussian distribution, as described in Eq. [S7] and as shown in Figs. 4B-C, S5B-C, and S7B-C. Peak position of the 2D Gaussian fitting curve for 20 precise locations of each NP was used to determine final precise location of each NP (SMNOBS) bound with single streptavidin molecules in single biotin-streptavidin complexes. Standard deviation of the precise location of each NP was determined using FWHM of the 2D Gaussian fitting curve, as described above in Eq. [S8].

Nanometer-Resolution Mapping of Individual Biotin Molecules and Their Binding Sites in Single Streptavidin-Biotin Complexes Using PHOTON

Streptavidin molecules were immobilized on microscopic slides by incubating the slides with streptavidin (0.25 mg/mL) for 60 min, and well rinsing the slides with the PBS buffer. The

slides coated with streptavidin were incubated with SMNOBS (5.3 nM) in the buffer for 1 h and well rinsed with the buffer. A microchamber was created by sandwiching the buffer between the slide and a microscope coverslip, as we described previously.[1, 5, 11, 14] Plasmonic images and LSPR spectra of single SMNOBS bound with single streptavidin molecules on the slide were imaged using DFOMS.

Stacks of the plasmonic images of single AgMMUA-Biotin-Streptavidin NPs were acquired from 420 to 720 nm at each nm (1 nm spectral resolution) with 100-ms exposure time using MSIS. The LSPR spectra of AgMMUA-Biotin-Streptavidin NPs were deconvoluted using individual LSPR spectrum of single AgMMUA-Biotin NPs via Cauchy-Lorentz distribution model (Figs. 3C, S4C, S6C), as described above. We then used PSF to determine the centroids (precise locations) of individual SMNOBS bound with single streptavidin molecules (Figs. 3D, S4D, S6D).

The processes were repeated twenty times for each binding complex (AgMMUA-Biotin-Streptavidin NPs) to generate the distribution of centroids of single SMNOBS in the complex (Figs. 4A, S5A, S7A). We then utilized 2D Gaussian to fit the distribution of centroids of each SMNOBS and to determine its precise locations at nm resolution (Figs. 4B-C, S5B, S7B), as described in SI.

We assembled the precise locations of single SMNOBS bound with single streptavidin molecules into super-resolution images at nm resolution (Figs. 4B-C, S5C, S7C). LSPR spectra of single SMNOBS bound with single streptavidin molecules at given precise positions determined using PHOTON were acquired to validate that their sum matched with the LSPR spectra of single AgMMUA-Biotin-Streptavidin NPs (Figs. 4D, S5D, S7D). Spatial and temporal resolutions of PHOTON were determined, as described in the text.

TEM samples with the same molar ratio of streptavidin to SMNOBS at 10 were prepared and imaged using HRTEM (JEOL JEM-2100F).

Data Analysis and Statistics

We characterized 100 of single NPs (Ag, AgMMUA, AgMMUA-Biotin NPs) for each measurement of sizes and shapes of single Ag NPs using HRTEM, and plasmonic images and LSPR spectra of single Ag, AgMMUA, AgMMUA-Biotin NPs using DFOMS, to gain sufficient statistics to determine their size distribution and LSPR spectra (color) distribution that represent NP suspension in bulk solution at the single NP level. More than 100 of single AgMMUA-Biotin-Streptavidin NPs were imaged using PHOTON and HRTEM to gain sufficient statistics for mapping locations of single SMNOBS and their binding sites in single streptavidin molecules. Three measurements were performed for each experiment.

B. Supplementary Figures and Figure Captions

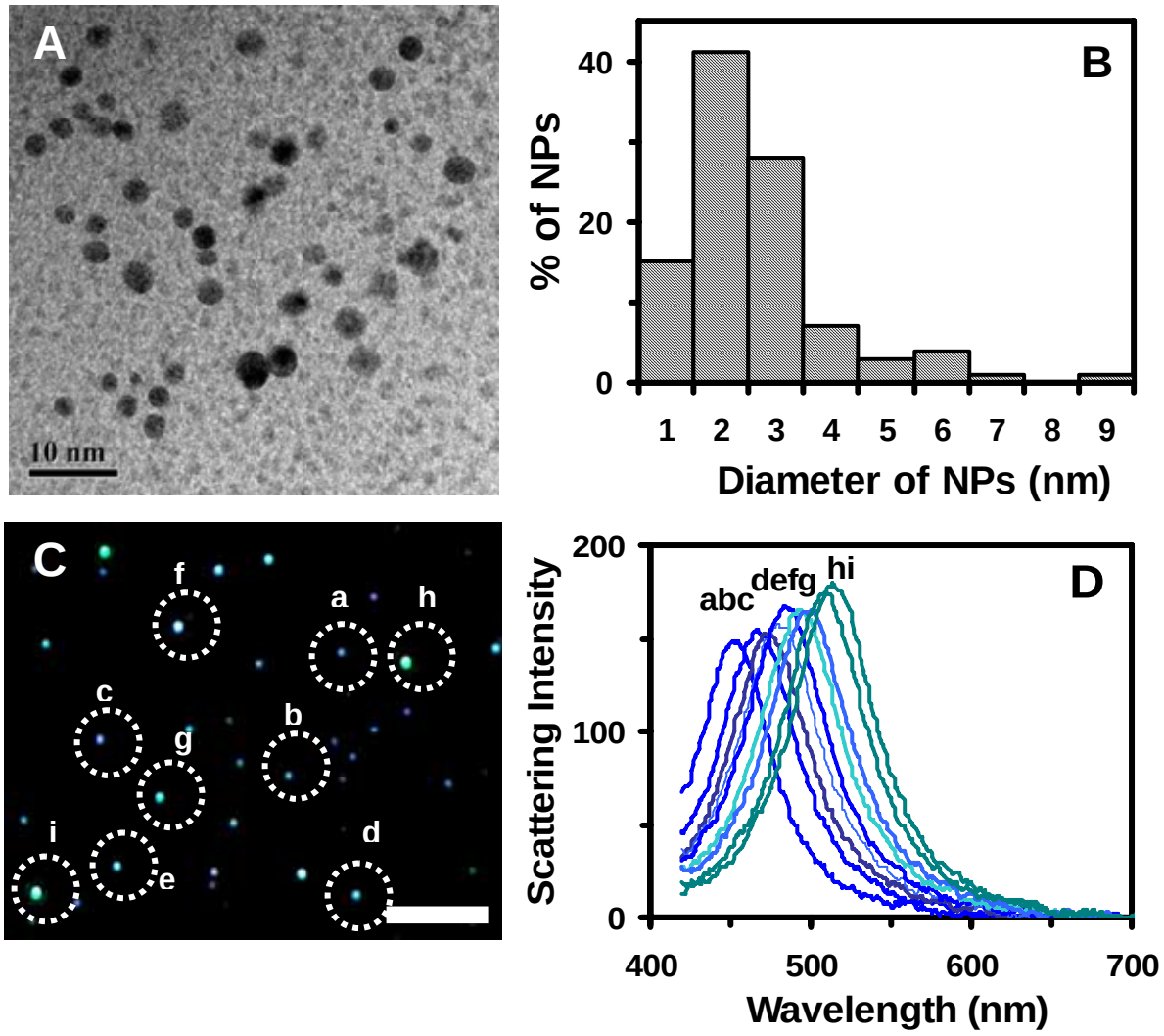

Fig. S1: Characterization of sizes and plasmonic optical properties of single Ag NPs: **(A)** HRTEM image of single Ag NPs and **(B)** Histogram of size distribution of single NPs show nearly spherical shape of NPs with average diameters of 2.6 ± 1.1 nm. **(C)** Dark field optical image and **(D)** LSPR spectra of single NPs show plasmonic blue and cyanic NPs with λ_{max} (FWHM) at (a) 450 (56), (b) 465 (60), (c) 472 (62), (d) 478 (64), (e) 482 (64), (f) 491 (64), (g) 496 (66), (h) 506 (64), and (i) 511 (65) nm, as circled in (C). Scale bars in (A) and (C) are 10 nm and 5 μm, respectively. The scale bar in (C) shows the distances between single NPs, but not the sizes of single NPs, because they are imaged under optical diffraction limit.

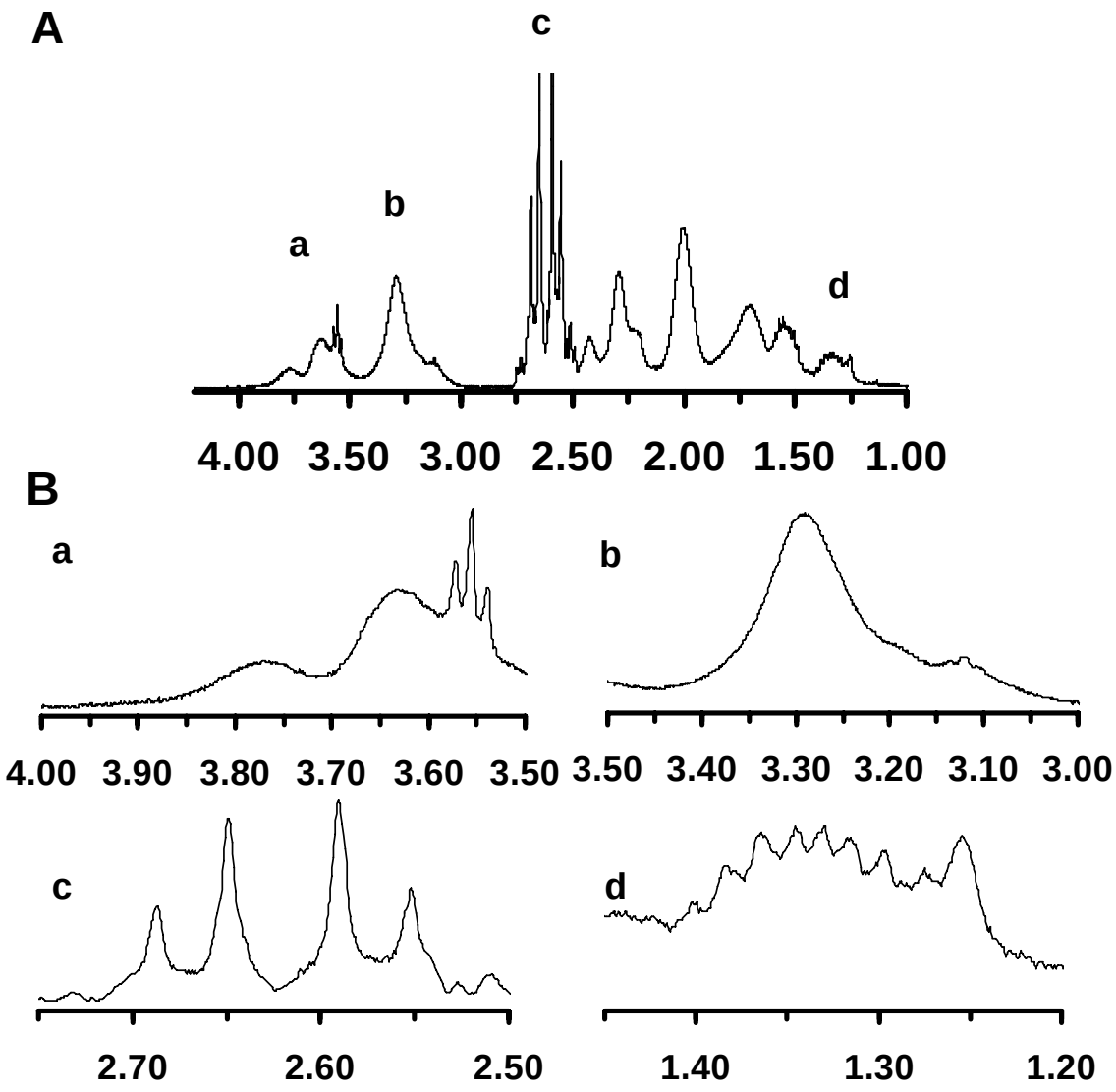

Fig. S2: NMR characterization of functional groups (citrate, MUA, MCH, PVP) attached on the surface of Ag NPs. **(A)** NMR spectra of AgMMUA NPs; **(B)** zoom-in individual peaks of NMR spectra in (A): (a) δ = 3.55 ppm, integration = 2.10, (**2H** in -(CH_2)-OH of MCH); (b) δ = 3.28 ppm, integration = 8.85, (**2H** from PVP ring); (c) δ = 2.62 ppm, integration = 28.03, (-C**H-**$_2$- next to thiol from both MUA and MCH and **4H** from citrate; (d) δ = 1.20-1.45 ppm, integration = 5.87, (**12H** from –$(CH_2)_2$-CH_2OH of MCH). Molar ratio of citrate : MCH : MUA : PVP = 33 : 5 : 1 : 0.03, showing a single carboxyl group per NP, as determined via a close-packing model.[1]

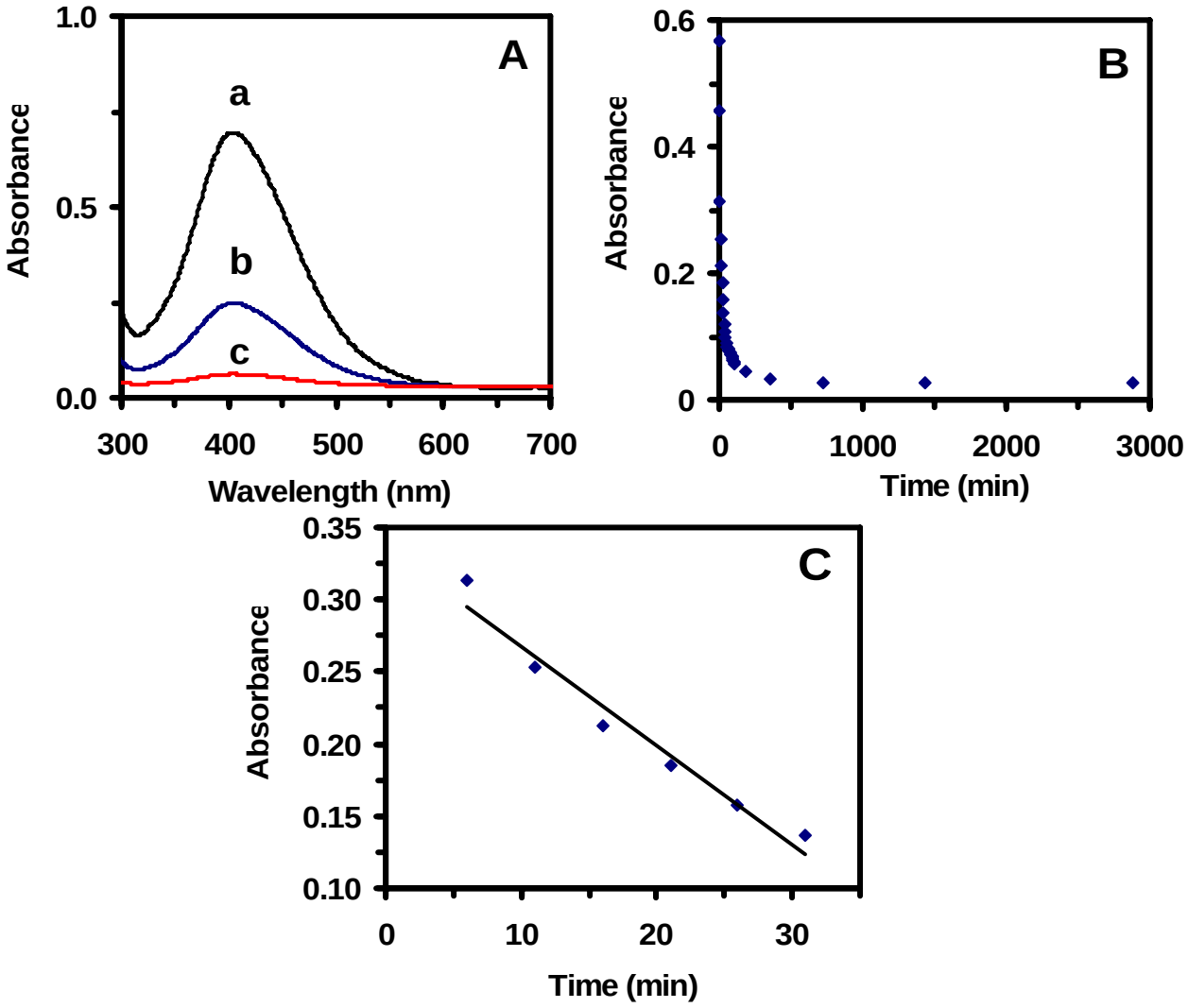

Fig. S3: Characterization of binding affinity and binding kinetics of AgMMUA-Biotin NPs (SMNOBS) with streptavidin: **(A)** UV-vis absorption spectra of 60 nM AgMMUA-Biotin NPs incubated with 600 nM streptavidin in PBS buffer (10 mM, pH 7.4) at (a) 0, (b) 21 min, and (c) 24 h, show that absorption peak wavelength at 403 ± 1 nm remains essentially unchanged, while the absorbance decreases with incubation time, suggesting that AgMMUA-Biotin NPs bound with streptavidin. **(B)** Plot of the peak absorbance corrected by baseline in (A) versus the incubation time, shows the exponential decay. **(C)** Zoom-in plot of (B) during 0 to 31 min, shows linearity with a slop of -6.8 x 10^{-3} min^{-1} and linear regression coefficient of determination (R^2) of 0.96. Binding constant ($3.2x10^{15}$) and associate rate constant ($6x10^2$ M^{-1} s^{-1}) are calculated using the approaches as we described previously.[1, 11]

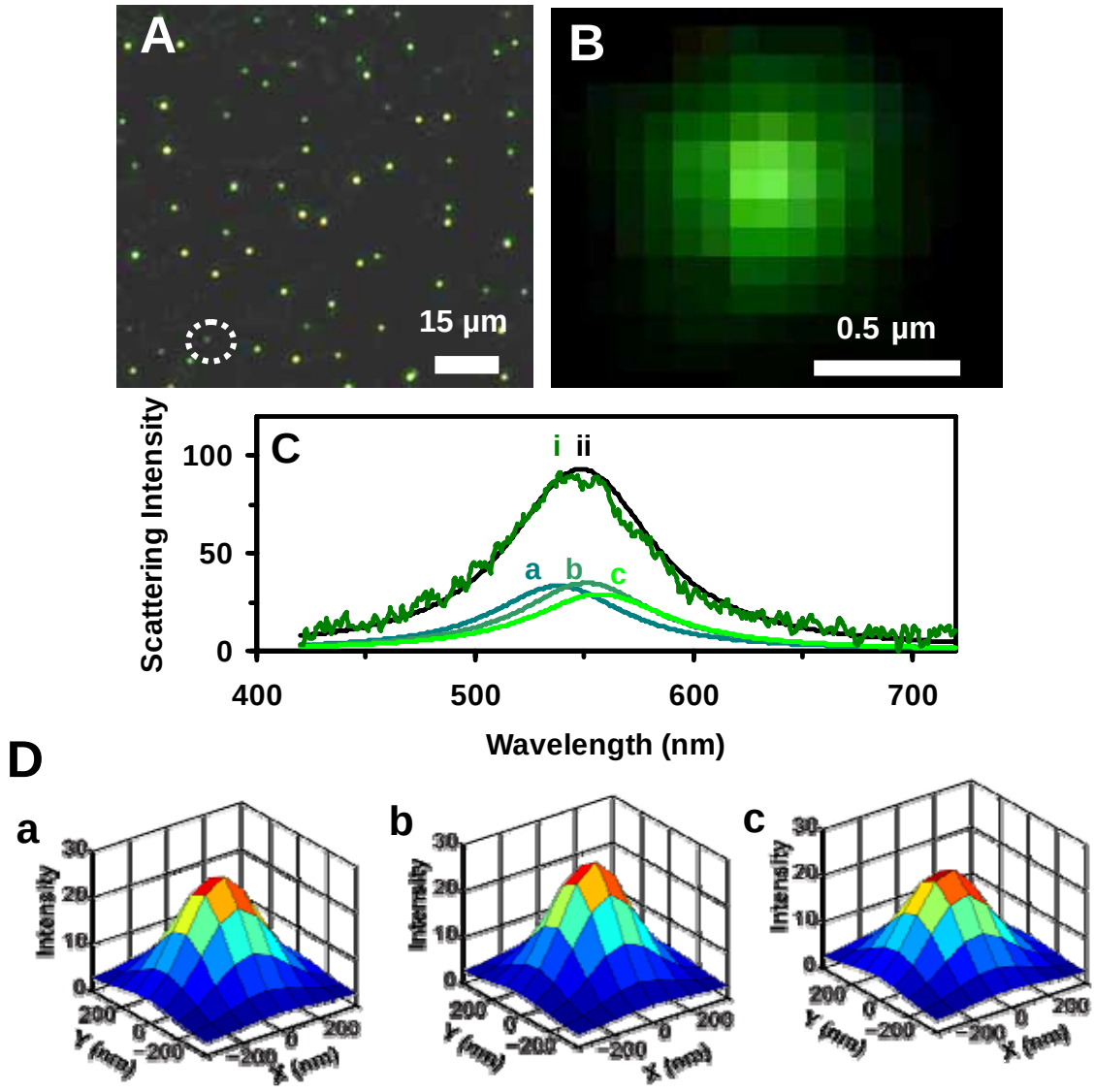

Fig. S4: Mapping of centroids of three SMNOBS bound with single streptavidin molecules using deconvolution and PSF. **(A)** Dark-field optical images of single AgMMUA-Biotin-Streptavidin NPs. **(B)** Zoom-in image of the NPs, circled in (A). **(C)**: (i) LSPR spectrum of the NPs in (B); (a-c) deconvoluted LSPR spectra of the spectrum in (i); and (ii) sum of deconvoluted LSPR spectra of (a-c), show λ_{max} (FWHM) at: (i) 547 (78); (ii) 548 (78); (a) 538 (68); (b) 551 (71); (c) 557 (66) nm. **(D)** Plots of scattering intensity of single SMNOBS with deconvoluted LSPR spectra of (a-c) in (C) versus their locations, respectively. As determined by PSF, the precise locations (centroids) of single AgMMUA-Biotin NPs bound with a streptavidin in (a-c) are (46.0, 64.0), (53.1, 59.2), (51.2, 51.2) nm, respectively. Scale bar in (A) and (B) are 15 and 0.5 μm, showing the distances between single NPs, but not the sizes of single NPs, due to optical diffraction limit.

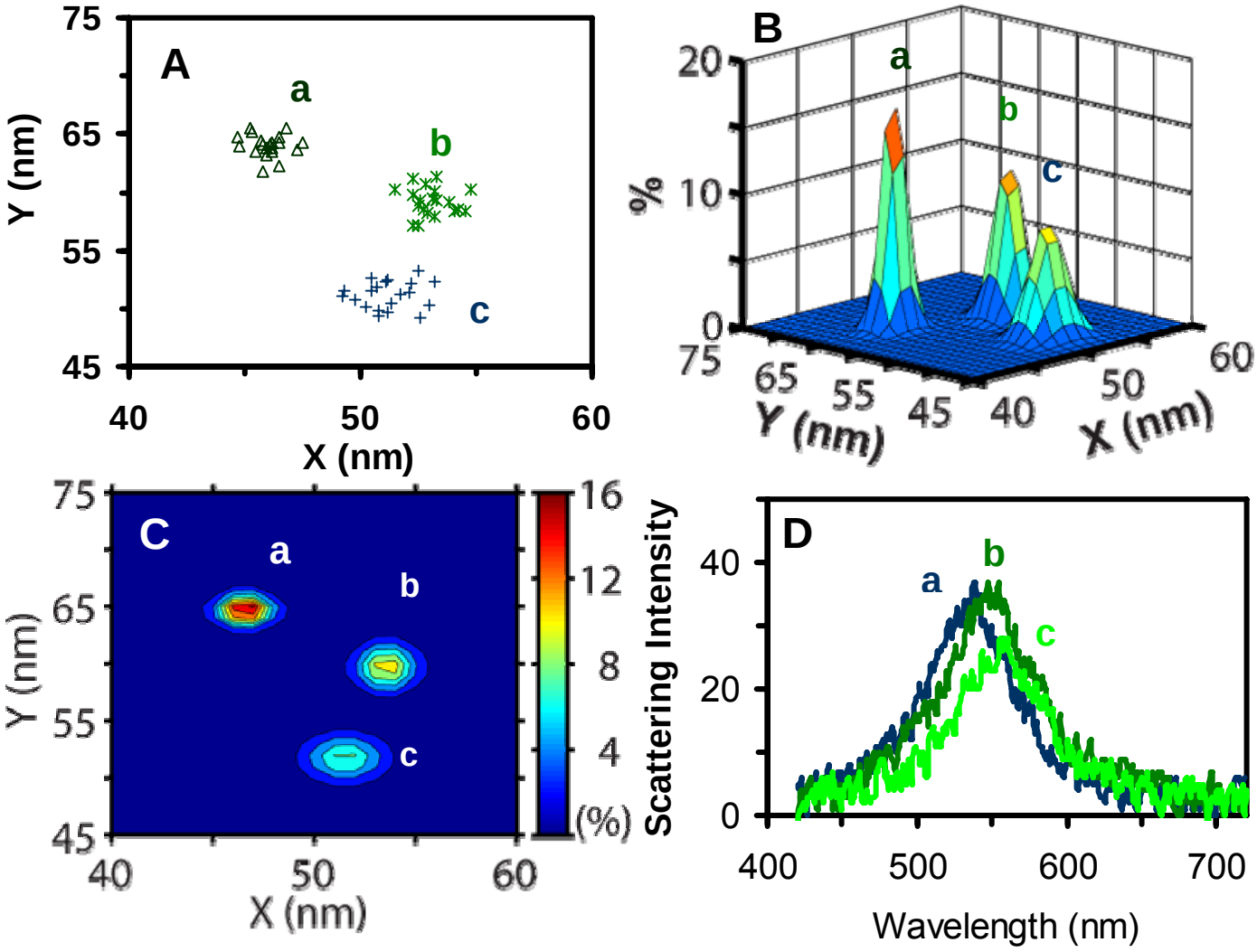

Fig. S5: Nanometer-resolution imaging of three SMNOBS bound with single streptavidin molecules (biotin-streptavidin complexes) using PHOTON. **(A)** Plots of distributions of precise locations (centroids) of single SMNOBS bound with a streptavidin molecule determined by PSF. Twenty repeated such measurements (points) are made for each NP. **(B)** 2D Gaussian fitting of the distributions of 20 precise locations of each NP in (A). **(C)** Contour plots of (B) show that centroids of single SMNOBS in (a-c) locate: at (46.0 ± 0.7, 64.0 ± 0.9); (52.1 ± 0.8, 59.2 ± 1.2); and (51.2 ± 1.1, 51.2 ± 1.2) nm, respectively. **(D)** LSPR spectra of single SMNOBS on the locations in (C) show λ_{max} (FWHM) at: (a) 538 (68); (b) 551 (71); and (c) 557 (66) nm, which agrees with deconvoluted LSPR spectra of single SMNOBS in Fig. S4C: a-c, respectively. Scale bar in (A) and (B) are 15 and 0.5 μm, showing the distances between single NPs, but not the sizes of single NPs, due to optical diffraction limit.

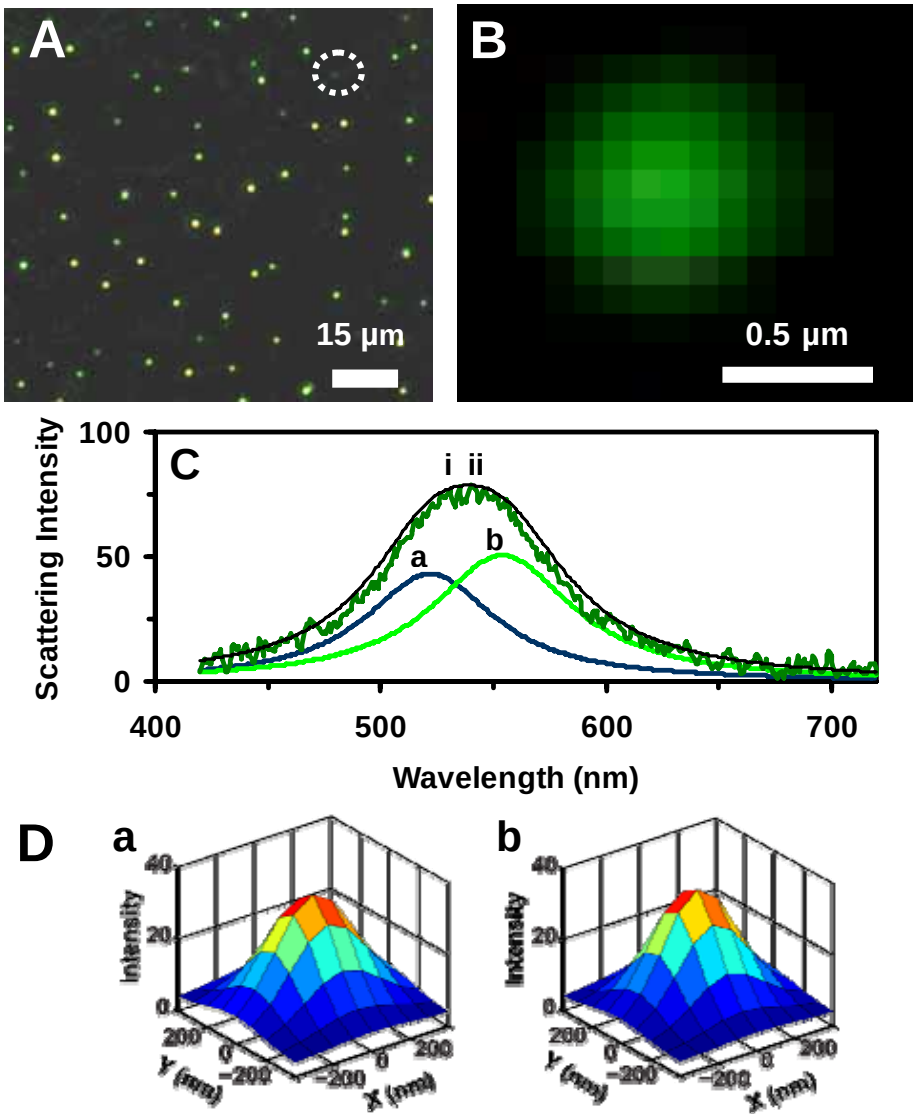

Fig. S6: Mapping of centroids of two SMNOBS bound with single streptavidin molecules using deconvolution and PSF. **(A)** Dark-field optical images of single AgMMUA-Biotin-Streptavidin NPs. **(B)** Zoom-in image of the NPs, circled in (A). **(C)**: (i) LSPR spectrum of the NPs in (B); (a-b) deconvoluted LSPR spectra of the spectrum in (i); and (ii) sum of deconvoluted LSPR spectra of (a-b), show λ_{max} (FWHM) at: (i) 540 (82); (ii) 540 (86); (a) 522 (62); (b) 554 (66) nm. **(D)** Plots of scattering intensity of single SMNOBS with deconvoluted LSPR spectra of (a-b) in (C) versus their locations, respectively. As determined by PSF, the precise locations (centroids) of single SMNOBS bound with a streptavidin in (a-b) are (41.9, 51.3), (45.0, 59.2) nm, respectively. Scale bar in (A) and (B) are 15 and 0.5 μm, showing the distances between single NPs, but not the sizes of single NPs, due to optical diffraction limit.

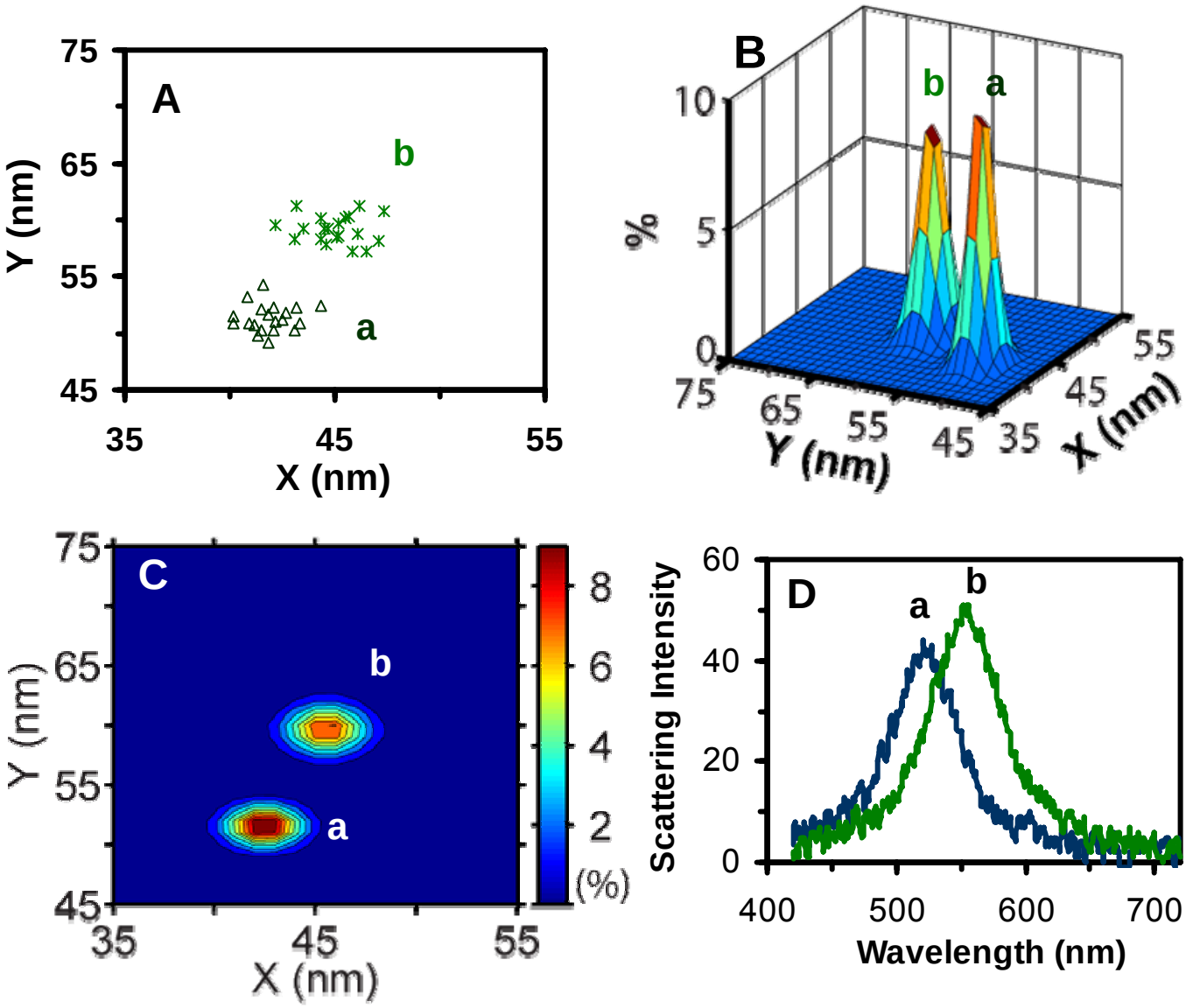

Fig. S7: Nanometer-resolution imaging of two SMNOBS bound with single streptavidin molecules (biotin-streptavidin complexes) using PHOTON. **(A)** Plots of distributions of centroids of single SMNOBS bound with a streptavidin molecule determined by PSF. Twenty repeated such measurements (points) are made for each NP. **(B)** 2D Gaussian fitting of the distributions of 20 precise locations of each SMNOBS in (A). **(C)** Contour plots of (B) show that centroids of single SMNOBS in (a-b) locate: at (41.9 ± 1.1, 51.3 ± 1.2) and (45.0 ± 1.3, 59.2 ± 1.2) nm, respectively. **(D)** LSPR spectra of single SMNOBS on the locations in (C) show λ_{max} (FWHM) at: (a) 522 (62) and (b) 554 (66) nm, which agrees with deconvoluted LSPR spectra of single SMNOBS in Fig. S6C: a-b, respectively.

References

1. T. Huang, P. D. Nallathamby and X.-H. N. Xu, *J. Am. Chem. Soc.* , 2008, **130**, 17095-17105.
2. T. Huang and X.-H. N. Xu, *J. Mater. Chem.* , 2010, **20**, 9867-9876
3. K. J. Lee, P. D. Nallathamby, L. M. Browning, C. J. Osgood and X.-H. N. Xu, *ACS Nano*, 2007, **1**, 133-143.
4. X.-H. N. Xu, S. Huang, W. Brownlow, K. Salatia and R. Jeffers, *J. Phys. Chem. B.* , 2004, **108**, 15543-15551.
5. P. D. Nallathamby, K. J. Lee, T. Desai and X.-H. N. Xu, *Biochemistry*, 2010, **49**, 5942-5953.
6. P. D. Nallathamby and X.-H. N. Xu, *Nanoscale*, 2010, **2**, 942-952.
7. X.-H. N. Xu, W. J. Brownlow, S. V. Kyriacou, Q. Wan and J. J. Viola, *Biochemistry*, 2004, **43**, 10400-10413.
8. L. M. Browning, K. J. Lee, T. Huang, P. D. Nallathamby, J. Lowman and X.-H. N. Xu, *Nanoscale*, 2009, **1**, 138-152.
9. P. D. Nallathamby, K. J. Lee and X.-H. N. Xu, *ACS Nano*, 2008, **2**, 1371-1380.
10. Y. Song, P. D. Nallathamby, T. Huang, H. Elsayled-Ali and X.-H. N. Xu, *J. Phys. Chem. C.*, 2010, **114**, 74-81.
11. T. Huang, P. D. Nallathamby, D. Gillet and X.-H. N. Xu, *Anal. Chem.*, 2007, **79**, 7708-7718.
12. S. V. Kyriacou, W. J. Brownlow and X. H. N. Xu, *Biochemistry*, 2004, **43**, 140-147.
13. S. V. Kyriacou, M. E. Nowak, W. J. Brownlow and X.-H. N. Xu, *J. Biomed. Opt.*, 2002, **7**, 576-586.
14. X.-H. N. Xu, J. Chen, R. B. Jeffers and S. V. Kyriacou, *Nano Lett.*, 2002, **2**, 175-182.
15. X.-H. N. Xu and R. P. Patel, in *Encyclopedia of Nanoscience and Nanotechnology*, ed. H. S. Nalwa, American Scientific Publishers, Stevenson Ranch, CA, 2004, vol. 7, pp. 189-192.
16. X.-H. N. Xu, Y. Song and P. D. Nallathamby, in *New Frontiers in Ultrasensitive Bioanalysis: Advanced Analytical Chemistry Applications in Nanobiotechnology, Single Molecule Detection, and Single Cell Analysis*, ed. X.-H. N. Xu, Wiley, New Jersey, 2007, pp. 41-65.
17. S. C. Gebhart, R. C. Thompson and A. Mahadevan-Jansen, *Appl. Opt.*, 2007, **46**, 1896-1910.
18. M. Gonzalez, L. A. Bagatolli, I. Echabe, J. L. R. Arrondo, C. E. Argarana, C. R. Cantor and G. D. Fidelio, *J. Biol. Chem.*, 1997, **272**, 11288-11294.
19. O. H. Laitinen, V. P. Hytönen, H. R. Nordlund and M. S. Kulomaa, *Cell Mol. Life Sci.* , 2006, **63**, 2992-3017.
20. W. A. Hendrickson, A. Pähler, J. L. Smith, Y. Satow, E. A. Merritt and R. P. Phizackerley, *Proc. Natl. Acad. Sci. U. S. A.* , 1989, **86**, 2190-2194.
21. A. Delaigle, P. Hall and A. Meister, *Ann Stat.* , 2008, **36**, 665-685.
22. R. D. B. Fraser and E. Suzuki, *Anal. Chem.*, 1969, **41**, 37-39.
23. T. Klar, M. Perner, S. Grosse, G. von Plessen, W. Spirkl and J. Feldmann, *Phys. Rev. Lett.*, 1998, **80**, 4249-4252.
24. V. D. Barnett, *J. Amer. Statist. Assoc.*, 1966, **61**, 1205-1218.
25. D. L. Farkas, C. Du, G. W. Fisher, C. Lau, W. Niu, E. S. Wachman and R. M. Levenson, *Comp. Med. Imag. Graph.*, 1998, **22**, 89-102.
26. R. E. Thompson, D. R. Larson and W. W. Webb, *Biophys. J.*, 2002, **82**, 2775-2783.